Voltage Behaviour in Radial Distribution Systems under the Uncertainties of Photovoltaic Systems and Electric Vehicle Charging Loads

F. J. Ruiz-Rodriguez[1], J. C. Hernández[2*], F. Jurado[3]

[1] *Department of Electrical and Thermal Engineering, University of Huelva, 21004 Spain*
[2] *Department of Electrical Engineering, University of Jaén, 23071 EPS Jaén, Spain*
[3] *Department of Electrical Engineering, University of Jaén, 23700 EPS Linares, Jaén, Spain*

SUMMARY

This paper presents a probabilistic method that accurately verifies the fulfilment of voltage constraints in radial distribution systems (RDSs) with photovoltaic (PV) systems and electric vehicle (EV) charging loads. This problem has not been comprehensively discussed. The proposed probabilistic method (PPM) involves the calculation of input variable cumulants, the linearization of load-flow equations, and the application of the cumulant method and the Cornish-Fisher expansion. Obviously, it is first necessary to model the PV systems and EV charging loads as random variables. In addition, the correlation of the input variables is suitably handled.

As part of this research, a Monte Carlo simulation (MCS) was performed, which confirmed the accuracy of the results obtained with the PPM. As an added value, when compared to the MCS, there was a significant reduction in computational cost.

The results obtained by the PPM demonstrate that the connection of PV systems in the IEEE 33-node RDS with EVs clearly contributes to keeping voltages within regulatory limits, once the distributions of the RDS output variables are inspected. Nonetheless, the greater dispersion in the distributions in combined PV and EV scenarios means that voltage constraint fulfilment cannot be absolutely guaranteed. This probabilistic approach provides a more accurate assessment than one based on a simple deterministic vision. Thus, the PPM is extremely useful because it provides a better

* Corresponding author. +34 953 21 24 63; fax: +34 953 21 24 78.
E-mail addresses: javier.ruiz@die.uhu.es (F.J. Ruiz-Rodriguez), jcasa@ujaen.es (J.C. Hernández), fjurado@ujaen.es (F. Jurado).

understanding of the combined technical impact under different correlated and uncorrelated scenarios.

KEY WORDS: Distribution radial systems; electric vehicles; load flow analysis; probability; photovoltaics.

1. INTRODUCTION

There is currently great concern regarding the possible effects of climate change. For this reason, international policy [1-3] increasingly envisages a reduction in the use of fossil fuels. Nevertheless, fossil fuels are still widely used to generate electricity and to power road vehicles. For this reason, the future trend in the electricity sector is a change to renewable power gradually, such as wind, PV, solar thermal, biomass, etc. [4]. Furthermore, the internal combustion engines of vehicles will eventually be replaced by motors, powered by electric batteries [5].

Numerous researchers have assessed the technical impacts of EVs on RDSs [5-13]. In a parallel way, other researchers have investigated the technical impacts of PV systems on RDSs [14-23]. The assessment of technical impact of PV systems and EVs has recently emerged in literature [24-32]. Nonetheless, up to the present, potentially negative technical impacts have been minimized by strict interconnection requirements (e.g. PV systems [33] and EVs [34]). Such requirements are based on a deterministic assessment in the form of worst-case scenarios, namely, average or peak load assessments. However, this type of evaluation is unable to objectively specify when an index that characterises the time-variant values of an RDS output variable (e.g. node voltage) can exceed the standard limit in the regulation. Examples of voltage limits include the following: -2.5/5% IEEE Std. 1547 [35], -5/5.8% ANSI Std. C84.1 [36], and ±10% EN 50160 [37]. Furthermore, it is also unable to determine the frequency of this event because the variables in an RDS with PV systems and EVs are subject to uncertainties stemming from the inherent randomness of PV power outputs and EV battery charging loads. Consequently, probabilistic techniques [38] are the key to a more accurate assessment of the combined impact of uncertainties regarding RDS output variables. Of these techniques, the ones that are most frequently used are the following: probabilistic load flow methods based on MCS [5- 11,13,20-22,26,27,31,39], analytical techniques [17,18,30], and approximation methods [19,28].

From the literature review about the impact of PV systems [5-13], EVs [14-23] or the combined interaction [24-32] on RDSs, major identified shortcomings in studies include: (i) the simulation step is not adjusted to 10-mins (usually 0.5 h or 1 h is planned); (ii) the technical impact is assessed without considering its probability of occurrence. This means that the probability distribution of the RDS output variable is not calculated; the averaged values are usually given and the probability of voltage threshold violation is not computed; (iii) the correlation of the input variables is rarely considered.

To the best of our knowledge, this research study is the first to present a method capable of assessing accurately the combined technical impact of the PV and EV uncertainties on RDSs. Thus, true probabilities of threshold violation in regulations are determined from probability distributions of the RDS output variables. This research thus complements the previous effort in [18] and formulates a PPM based on an analytical technique that is computationally more effective than the mainstream MCS. The remainder of this paper is organized as follows. Section 2 presents the statistical background. Section 3 provides an overview of probabilistic models. Section 4 shows the correlation of the input variables. Section 5 describes the method created in this study. Section 6 presents the simulation results and verifies the fulfilment of voltage constraints in a test RDS in different scenarios. Finally, section 7 summarizes the main conclusions derived from this research.

2. MOMENTS AND CUMULANTS OF RANDOM VARIABLES

The moments of a random variable are descriptive measurements that reveal the properties of the variable and determine its distribution function [40-42]. For a multivariable random variable $\boldsymbol{X}\,(=[\boldsymbol{X}_1,\boldsymbol{X}_2,...,\boldsymbol{X}_{N_{rv}}]^{\mathrm{T}})$ with PDF $f_{\boldsymbol{X}}(\boldsymbol{X})$ (continuous variable), or with PMF $f^{*}_{\boldsymbol{X}}(\boldsymbol{X})$ (discrete variable), its *r*th-order moment is defined as [40-42]:

$$\alpha_{\boldsymbol{X}}^{i_1\ldots i_r\,(r)}=\mathrm{E}\left[X_{i_1}\cdot\ldots\cdot X_{i_r}\right]=\int_{-\infty}^{\infty}\ldots\int_{-\infty}^{\infty}X_{i_1}\cdot\ldots\cdot X_{i_r}\cdot f_{\boldsymbol{X}}(\boldsymbol{X})\,d\boldsymbol{X};$$
$$\alpha_{\boldsymbol{X}}^{i_1\ldots i_r\,(r)}=\sum_{i_1=1}^{\infty}\ldots\sum_{i_r=1}^{\infty}X_{i_1}\cdot\ldots\cdot X_{i_r}\cdot f^{*}_{\boldsymbol{X}}(\boldsymbol{X}) \tag{1}$$

Cumulants are also descriptive measurements that reveal the properties of a random variable [42]. Even though moments $\alpha_{\boldsymbol{X}}^{i_1\ldots i_r\,(r)}$ and cumulants $\kappa_{\boldsymbol{X}}^{i_1\ldots i_r\,(r)}$ are related [41,42],

cumulants have properties that make their manipulation even easier when they are applied to a linear combination of random variables [40]. Thus, let $\boldsymbol{Z}$ be a random variable that is a linear combination of a multivariate random variable, $\boldsymbol{X}$, given by:

$$\boldsymbol{Z} = \sum_{i=1}^{N_{rv}} a_i \cdot \boldsymbol{X_i} \tag{2}$$

Applying the cumulant method [40], for example, the third-order cumulant of the random variable $\boldsymbol{Z}$ can be expressed as a function of the cumulants of the variable $\boldsymbol{X}$ as:

$$\kappa_{\boldsymbol{Z}}^{111} = \sum_{i=1}^{N_{rv}} \sum_{j=1}^{N_{rv}} \sum_{k=1}^{N_{rv}} a_i a_j a_k \kappa_{\boldsymbol{X}}^{ijk} \tag{3}$$

In general, the cumulant of order *r* could be obtained as [40]:

$$\kappa_{\boldsymbol{Z}}^{r\,1\ldots1} = \sum_{i_1=1}^{N_{rv}} \overset{r}{\cdots} \sum_{i_r=1}^{N_{rv}} a_{i_1}^{\;r} \cdots a_{i_r} \cdot \kappa_{\boldsymbol{X}}^{r\,i_1\ldots i_r} \tag{4}$$

3. PROBABILISTIC MODELS

3.1. PV system model

The modelling of the AC output power in a PV system is based on meteorological random variables. A detailed time-varying model description is presented in [43]. The model is used to obtain the PV random power for each *x*th10-min interval of the day (t_x), *m*th month, and *n*th RDS node $\boldsymbol{p}_{pv,n,10\text{-}min_{t_x}}^{m}$ as a linear combination of the meteorological random variables $\boldsymbol{K}_{\boldsymbol{t,n}}^{m}$ (daily clearness index) and $\boldsymbol{k}_{\boldsymbol{d,n}}^{m}$ (hourly diffuse fraction) [43]:

$$\boldsymbol{p}_{pv,n,10\text{-}min_{t_x}}^{m} = a_1 + a_2 \cdot \boldsymbol{K}_{\boldsymbol{t,n}}^{m} + a_3 \cdot \boldsymbol{k}_{\boldsymbol{d,n}}^{m} \tag{5}$$

Random variables $\boldsymbol{K}_{\boldsymbol{t,n}}^{m}$ and $\boldsymbol{k}_{\boldsymbol{d,n}}^{m}$ take both the global and diffuse irradiation into account; they depend on the day of the year and the geographical location. A detailed description of how these variables are obtained as well as coefficients a_1, a_2 and a_3 can be found in [43].

The PV model determines the cumulants of $\boldsymbol{p}_{pv,n,10\text{-}min_{t_x}}^{m}$ from cumulants of meteorological random variables. Then, series expansion [17,18,44] provides the statistical characterization (PDF, CDF) of the $\boldsymbol{p}_{pv,n,10\text{-}min_{t_x}}^{m}$.

Under the recommendation of IEEE Std. 1547 [35], PV inverters are not permitted to generate reactive power to the grid. Furthermore, grid requirements for PV systems

connected to distribution or transmission systems [33] force the participation in the reactive power control when PV power surpasses at least 1 MW. Accordingly, PV systems in this study, only inject active power and do not control the node voltage.

3.2. Time-varying load model

When analysing the daily load profile of an RDS node based on 10-min measurements for the one-year time period, measurements usually fall in a small region around the time-conditional mean. This is due to the dependence of the human activities on a cyclic-deterministic phenomenon (time of day, day of week, season) [45,46]; the power consumption is not so stochastic, but presents a high time-dependence. This time-dependence can be removed by performing the calculation separately for groups of time periods (e.g. 10-min interval, 1 hour) with similar statistical characteristics (time-frames analysis [47]).Thus, the load in each time-frame can be modelled by superimposing a random noise variable to the time-conditional mean. This has been the basic load modeling platform in power systems analysis. The usual practice is to use a normal distribution for modeling the load stochasticity in each time-frame.

From daily typical profiles based on historical statistical data [15], it is possible to statistically characterize (PDF, CDF) the active or reactive random load for each *x*th10-min interval of the day (t_x) - time-frame chosen -, *m*th month, and *n*th RDS node $\boldsymbol{p}^{m}_{l,n,10\text{-}min_{t_x}}$ ($\boldsymbol{q}^{m}_{l,n,10\text{-}min_{t_x}}$) according to [17,18]. Obviously, due to the time-dependant nature of loads, each 10-min interval of the day has a different normal distribution.

3.3. Model of time-varying EV charging load

The EV charging load should be determined by a minimum of three random variables: (i) the charging start time ($\boldsymbol{t_k}$); (ii) the initial SOC of the EV battery (***E)***; and (iii) the EV battery charging characteristics, which may vary, depending on battery type and charging mode. For example, Figure 1 depicts the generic charging profile and SOC for lithium-ion batteries [11,48].

Figure 1**.** Generic charging profile and SOC for lithium-ion batteries.

Typical values of the parameters for charging an EV supplied by a battery pack of 25 kWh for the four standard modes in IEC 61851-1 [49] are depicted in Table I.

Table I. Parameters of EV battery charging profile.

The initial SOC of the EV battery depends on the EV use. In addition, it can be assumed to be a random variable, depending on the distance travelled. Usually, the random variable distance $\boldsymbol{d}$ is represented by a lognormal type distribution [12]. The PDF is given by:

$$f_{\boldsymbol{d}}\left(\boldsymbol{d};\mu_{\boldsymbol{d}},\sigma_{\boldsymbol{d}}\right)=\frac{1}{\boldsymbol{d}\cdot\sigma_{\boldsymbol{d}}\sqrt{2\pi}}e^{-\frac{\left(\ln\boldsymbol{d}-\mu_{\boldsymbol{d}}\right)^2}{2\sigma_{\boldsymbol{d}}{}^2}};\quad \boldsymbol{d}>0 \tag{6}$$

Taking into account the daily distance driven by an EV, $\boldsymbol{E}$ (the initial SOC of the EV battery) at the beginning of a recharge cycle can be expressed by:

$$\boldsymbol{E}=1-\frac{\boldsymbol{d}}{d_r};\quad 0<\boldsymbol{d}<d_r \tag{7}$$

Bearing in mind the transformation theorem of random variables in (6) and (7), the resulting PDF for the random variable, $\boldsymbol{E}$ **(**initial SOC of the EV battery)**,** is given for one-day trip by:

$$f_{\boldsymbol{E}}\left(\boldsymbol{E};\mu_{\boldsymbol{d}},\sigma_{\boldsymbol{d}}\right)=\frac{1}{\left(1-\boldsymbol{E}\right)\cdot\sigma_{\boldsymbol{d}}\sqrt{2\pi}}e^{-\frac{\left(\ln(1-\boldsymbol{E})+\ln d_r-\mu_{\boldsymbol{d}}\right)^2}{2\sigma_{\boldsymbol{d}}{}^2}};\quad 0<\boldsymbol{E}<1 \tag{8}$$

To simplify the calculations, the continuous charging power $(p_{ev}^{\Diamond})$ shown in Figure 1 is discretized into 10-min predefined intervals. Thus, the corresponding discrete charging power level for the *j*th 10-min interval $p_{ev,10\text{-}min_j}$ can be expressed by:

$$p_{ev,10\text{-}min_j}=\frac{1}{T}\int_{t_{j-1}}^{t_j}p_{ev}^{\Diamond}(t)dt;\quad 1\le j\le N_c \tag{9}$$

Each discrete power level $p_{ev,10\text{-}min_j}$ corresponds to a discrete SOC of the EV battery $E_{10\text{-}min_j}$ (Figure 1). Let us assume that an EV battery with a SOC $E_{10\text{-}min_j}$ is charged at time t_j and that the charging power is $p_{ev,10\text{-}min_j}$. If the charging process starts at an earlier time $t_{x\text{-}k}$ of t_j, ($k \le x$), then at time t_k, the SOC of the EV battery is $E_{10\text{-}min_{j\text{-}(x\text{-}k)}}$ and the charging power level is $p_{ev,10\text{-}min_{j-(x-k)}}$.

The random variables charging start time $\boldsymbol{t_k}$, and initial SOC of the EV battery $\boldsymbol{E}$ are usually assumed to be independent variables [11,12]. Accordingly, the singleton probability φ that the random variable, $\boldsymbol{p}_{\boldsymbol{ev,n,10\text{-}min_{t_x}}}^{\boldsymbol{m}}$, the charging power of an EV at any

*x*th 10-min interval of the day (t_x), *m*th month, and *n*th RDS node ($n = 1,...,N_{ev}$), will operate at charging power level $p_{ev,10\text{-}min_j}$ can be expressed as:

$$\varphi^{m}_{n,10\text{-}min_{t_x}}(p_{ev,10\text{-}min_j}) = \sum_{k=1}^{x} f_{\boldsymbol{E}}(\boldsymbol{E}_{\boldsymbol{10\text{-}min_{j\text{-}(x\text{-}k)}}}) \cdot h^{m}_{\boldsymbol{t_k},n}(\boldsymbol{t_k}); \quad N_c \le x \le 144; \quad x-k<j; \ \text{x<j} \qquad (10)$$

For domestic customers, the random variable $\boldsymbol{t_k}$ can be considered as a normal random variable [5].

From (1) and (10), for the *m*th month at any *x*th 10-min interval (t_x), and *n*th RDS node, the expected value and standard deviation of the random variable, $\boldsymbol{p^{m}_{ev,n,10\text{-}min_{t_x}}}$ can be obtained as follows:

$$\begin{aligned} \mu_{\boldsymbol{p^{m}_{ev,n,10\text{-}min_{t_x}}}} &= \sum_{j=1}^{N_c} p_{ev,10\text{-}min_j} \cdot \varphi^{m}_{n,10\text{-}min_{t_x}}(p_{ev,10\text{-}min_j}) \\ \sigma_{\boldsymbol{p^{m}_{ev,n,10\text{-}min_{t_x}}}} &= \sqrt{\sum_{j=1}^{N_c}\left[p_{ev,10\text{-}min_j} - \mu_{\boldsymbol{p^{m}_{ev,n,10\text{-}min_{t_x}}}}\right]^2 \cdot \varphi^{m}_{n,10\text{-}min_{t_x}}(p_{ev,10\text{-}min_j})} \end{aligned} \qquad (11)$$

According to the Central limit theorem, as the number of independent random variables involved increases, the distribution of the sum of these random variables tends to a normal distribution with a mean and variance, regardless of the original probability distribution. Therefore, given a set λ of EVs with the same EV battery charging profile, the expected value and standard deviation of the normal random variable representing the charging power of the whole EVs, $\boldsymbol{p^{m}_{wev,n,10\text{-}min_{t_x}}}$ in the *m*th month at any *x*th 10-min interval (t_x), and *n*th RDS node is given by:

$$\begin{aligned} \mu_{\boldsymbol{p^{m}_{wev,n,10\text{-}min_{t_x}}}} &= \lambda \cdot \mu_{\boldsymbol{p^{m}_{ev,n,10\text{-}min_{t_x}}}} \\ \sigma_{\boldsymbol{p^{m}_{wev,n,10\text{-}min_{t_x}}}} &= \sqrt{\lambda \cdot \left(\sigma_{\boldsymbol{p^{m}_{ev,n,10\text{-}min_{t_x}}}}\right)^2} \end{aligned} \qquad (12)$$

4. CHARACTERIZATION OF THE CORRELATION AMONG INPUT VARIABLES

Each RDS input variable $\boldsymbol{X_i}$ may or may not be correlated with each other. Generally speaking, the correlation is stated through the correlation coefficient matrix $\sum_{\boldsymbol{X}}$. The *ij*th element of $\sum_{\boldsymbol{X}}$ is [50]:

$$\rho_{X_i,X_j} = \frac{\mathrm{cov}(\boldsymbol{X}_i, \boldsymbol{X}_j)}{\sigma_{\boldsymbol{X}_i}\sigma_{\boldsymbol{X}_j}} = \frac{\mathrm{E}\left[\left(X_i - \mu_{\boldsymbol{X}_i}\right)\left(X_j - \mu_{\boldsymbol{X}_j}\right)\right]}{\sigma_{\boldsymbol{X}_i}\sigma_{\boldsymbol{X}_j}} \qquad (13)$$

For the RDS nodes, the load correlation due to cyclic-human activities is reasonable [51]. Also, PV generations are correlated because of common factors such as weather conditions [52].

When the individual random variables of interest have different marginal distributions, a multivariate joint distribution function can be created using a copula function [53,54], which represents the correlation structure between variables. A copula is a function that joins univariate distribution functions to form multivariate distribution functions. Thus, the random variables $\boldsymbol{X_i}$, $(i=1,...,N_{rv})$, with CDFs $F_{X_i}(\boldsymbol{X_i})$, are joined by copula *COP* if their joint distribution function $F_{\boldsymbol{COP}} = F_{X_1,X_2,...,X_{N_{rv}}}$ can be expressed as:

$$F_{\boldsymbol{COP}}(\boldsymbol{X_1},\boldsymbol{X_2},...,\boldsymbol{X}_{N_{rv}}) = F_{X_1,X_2,...,X_{N_{rv}}}[F_{X_1}^{-1}(\boldsymbol{U_1}),F_{X_2}^{-1}(\boldsymbol{U_2}),...,F_{X_{N_{rv}}}^{-1}(\boldsymbol{U}_{N_{rv}})] \quad (14)$$

4.1.1. Generation of correlated input samples using a Copula function

The method used to generate correlated inputs is based on the generation of multivariate correlated random numbers [53,54]. These numbers are used to numerically obtain both the non-crossed and crossed moments/cumulants required in the PPM, and also to run the MCS process that checks the results of the PPM. Summarising, the methodology in [53,54] is composed of the following steps:

Step 1) Transform random variables $\boldsymbol{X_i}$ to uniform variables using their CDFs:

$$\boldsymbol{U}_{X_i} = F_{X_i}(\boldsymbol{X}_i) \quad (15)$$

Step 2) Transform uniform variables $\boldsymbol{U}_{X_i}$ to normal variables using an inverse standard normal distribution (Nataf transformation):

$$\boldsymbol{W}_{X_i} = \phi^{-1}(\boldsymbol{U}_{X_i}) \quad (16)$$

Step 3) Estimate the correlation matrix $\sum_{W_X}$ of $\boldsymbol{W_X}$ from the known correlation matrix $\sum_{X}$ of input vector $\boldsymbol{X}$ [55-58]. The Gauss-Hermite quadrature in [59] can be used for this purpose.

Step 4) Generation of n_s correlated random input samples from a multivariate standard normal distribution $\boldsymbol{W_X}$ with a given correlation matrix $\sum_{W_X}$, forming the arrays $W_{X_1} \in \Re^{N_{pv}+N_l,n_s}$. Each element can be written as $W_{X_{1,ij}}$.

Step 5) Transform the generated values $W_{X_{1,ij}}$ back to the uniform domain $\boldsymbol{U}_{X_1}$ by applying the standard normal CDF as follows [58]:

$$\boldsymbol{U}_{\boldsymbol{X}_{1,i}} = \phi(W_{\boldsymbol{X}_{1,i}}) \tag{17}$$

Step 6) Transform the generated uniform values back to the original domain $\boldsymbol{X}_{1,i}$ by applying the inverse of the respective CDF:

$$\boldsymbol{X}_{1,i} = F_{X_i}^{-1}(\boldsymbol{U}_{\boldsymbol{X}_{1,i}}) \tag{18}$$

5. PROPOSED PROBABILISTIC METHOD TO ASSESS THE IMPACT OF PV SYSTEMS AND EVS ON RDSS

Figure 2 shows a flowchart of the PPM whereby the combined technical impact of PV systems and EVs on RDSs is assessed. This method is explained in the following sections. To summarise, firstly distributions (PDF or PMF and CDF) of RSD input random variables for one *x*th 10-min interval of the day (t_x) are determined according to section 3. In case of correlated scenarios, correlated input samples of PV powers and node loads are generated (see section 4.1.1). These samples, or the distributions in case of EVs, are used to determine the moments and cumulants of random inputs according to section 2. However, distributions directly determine moments and cumulants for uncorrelated scenarios. Subsequently, a deterministic radial load flow (section 5.1), determines the expected values of the output random variables. Taking the cumulants of input random variables into account, the probabilistic radial load flow in section 5.2 provides the PDF - $f_{u/\delta^m_{n,\ 10\text{-min}\,t_x}}$ - and the CDF - $F_{u/\delta^m_{n,\ 10\text{-min}\,t_x}}$ - of the nodal voltage angle and magnitude (at each *n*th RDS node in the *m*th month, and at the *x*th 10-min interval (t_x)).

Figure 2. Flowchart of the PPM to assess the impact of PV systems and EVs on RDSs.

5.1. Deterministic radial load flow

Nonlinear equations in (19) present the mathematical model in equilibrium at a steady state between the consumed and generated power in a power system with PV generation and EV charging loads:

$$\begin{aligned} p_n &= p_{g,n} + p_{pv,n} - p_{l,n} - p_{wev,n} = u_n \sum_{j=1}^{N_n} \left[u_j \left(g_{nj} \cos\delta_{nj} + b_{nj} sin\delta_{nj} \right) \right]; \\ q_n &= q_{g,i} - q_{l,i} \qquad\qquad = u_n \sum_{j=1}^{N_n} \left[u_j \left(g_{nj} sin\delta_{nj} - b_{nj} \cos\delta_{nj} \right) \right]; \qquad n = 1,...,N_n \end{aligned} \tag{19}$$

The Newton-Raphson algorithm applied to resolve the load flow in (19) causes some convergence problems in RDSs. Consequently, the alternative algorithm in [60], based on the application of Kirchhoff's laws, is used to solve the deterministic radial load

flow. More specifically, this algorithm provides the expected values of output random variables ($\mu_{u^m_{n,10\text{-}min_{t_x}}}$, $\mu_{\delta^m_{n,10\text{-}min_{t_x}}}$) from the expected input values, Figure 2. This algorithm is described in the following subsections.

5.1.1. Line numbering

The algorithm followed is line-oriented. Thus, a typical RDS has N_n nodes, f = (N_n-1) lines, and a voltage source in the root node. In this branched structure [60], the closest node in a line L_f to the root node is called L_1 and the farthest is named L_2.

5.1.2. Description of the algorithm

The algorithm begins by assuming that the entire RDS has a flat voltage profile, except for the root node, which has a rated voltage. The following iterative process then continues:

a. *Calculation of the current at each node:* at the *k*th iteration, the injection of current at each *n*th node $i_n^{(k)}$ is:

$$i_n^{(k)} = \left[\frac{s_n}{u_n^{(k-1)}}\right]^* - y_n \cdot u_n^{(k-1)} \tag{20}$$

b. *Backward movement:* at the *k*th iteration, starting from the lines in the last level and going in the direction of the lines related to the root node, the current in line L_f, $j^{L_f,(k)}$, is as follows:

$$j^{L_f,(k)} = -i_{L_2}^{L_f,(k)} + \sum\begin{pmatrix}\text{Current in branches}\\ \text{emanating from node } L_2\end{pmatrix} \tag{21}$$

c. *Forward sweep:* The voltages at the nodes are updated in this step, starting from the lines in the first level in the direction of those in the last. For each line, L_f, the voltage at node L_2 is calculated with the modified voltage at node L_1:

$$u_{L_2}^{L_f,(k)} = u_{L_1}^{L_f,(k)} - z^{L_f} \cdot j^{L_f,(k)} \tag{22}$$

Points a, b, and c are repeated until convergence is attained.

5.1.3. Verification of the convergence criterion

The convergence calculation is based on the active and reactive power mismatches at the nodes. The apparent power at the *k*th iteration for *n*th node, $s_n^{(k)}$ is given by:

$$s_n^{(k)} = u_n^{(k)} \left(i_n^{(k)} \right)^* - y_n^{(k)} \left| u_n^{(k)} \right|^2 \tag{23}$$

The reactive and real power mismatches at each *n*th node are:

$$\begin{aligned} \Delta p_n^{(k)} &= \mathrm{Re} \left| s_n^{(k)} - s_n \right| \\ \Delta q_n^{(k)} &= Im \left| s_n^{(k)} - s_n \right| \end{aligned} \tag{24}$$

In order to fulfil the convergence criterion, the largest mismatch in equation (24) must be less than a specified tolerance. The tolerance value is usually set at 10^{-6} p.u.

5.2. Probabilistic radial load flow

As certain input variables of an RDS with PV systems and EVs are subjected to uncertainties, a good way to characterise the sources of uncertainty is to represent these data as random variables. Although the MCS is simpler and directly uses many deterministic radial load flows, our proposal is based on an analytical technique that is computationally more effective than the MCS [18]. This first involves the linearization of load-flow equations (19), and second, it involves the application of the cumulant method [40] to determine the cumulants of output variables (see Figure 2). Once these cumulants are known, the PDF and CDF of the output variables (i.e. nodal voltage angles and magnitudes) are reconstructed by using the Cornish-Fisher expansion [44].

5.2.1. Linearization of load-flow equations

The linearization of the load-flow equations (19) allows obtaining the output random variables of the RDS as a linear combination (weighted sum) of the RDS random inputs. The linearization is performed around an operating point which matches to the expected values of the RDS random outputs that were obtained by the method presented in section 5.1.

To explain the linearization technique, let $\boldsymbol{A}$ and $\boldsymbol{B}$ be two random variables, and let $\boldsymbol{Y}$ be a third random variable $(\boldsymbol{Y} = \boldsymbol{A} \cdot \boldsymbol{B})$. If the deviations of $\boldsymbol{A}$ and $\boldsymbol{B}$ around their expected values $(\mu_{\boldsymbol{A}},\ \mu_{\boldsymbol{B}})$ are $\Delta\boldsymbol{A}$ and $\Delta\boldsymbol{B}$, respectively, it can be assumed that:

$$\boldsymbol{A} \approx \mu_{\boldsymbol{A}} + \Delta\boldsymbol{A}; \quad \boldsymbol{B} \approx \mu_{\boldsymbol{B}} + \Delta\boldsymbol{B} \tag{25}$$

When second-order terms are neglected $(\Delta\boldsymbol{A} \cdot \Delta\boldsymbol{B})$, the following expression is obtained:

$$\boldsymbol{Y} \approx \mu_{\boldsymbol{B}} \cdot \Delta\boldsymbol{A} + \mu_{\boldsymbol{A}} \cdot \Delta\boldsymbol{B} + \mu_{\boldsymbol{A}}\mu_{\boldsymbol{B}} = \mu_{\boldsymbol{B}} \cdot \boldsymbol{A} + \mu_{\boldsymbol{A}} \cdot \boldsymbol{B} - \mu_{\boldsymbol{A}}\mu_{\boldsymbol{B}} \tag{26}$$

This approximation is accurate for cases where the dispersion of the random variables is limited around the mean value. When this is not the case, the variable data will be processed less accurately.

This linearization technique is applied to the product of voltage magnitudes in equation (19) as follows:

$$\begin{aligned} u_n u_j &\approx \mu_{u_n} u_j + \mu_{u_j} u_n - \mu_{u_n}\mu_{u_j} \\ u_n^2 &\approx 2\mu_{u_n} u_j - \mu_{u_n}^2 \end{aligned} \tag{27}$$

For angles δ_{nj} in equation (19), the Maclaurin series are firstly applied on sine and cosine functions, and then the linearization is completed by the linear approximations [61]:

$$\begin{aligned} &\sin\delta_{nj} \approx \delta_{nj} - \frac{\delta_{nj}^3}{6}; \quad \rightarrow \quad \delta_{nj} - \frac{\delta_{nj}^3}{6} = a_{nj} + b_{nj}\delta_{nj}; \qquad (e.g.\ a_{nj} = 1 + \mu_{\delta_{nj}}^2/2) \\ &\cos\delta_{nj} \approx 1 - \frac{\delta_{nj}^2}{2}; \quad \rightarrow \quad 1 - \frac{\delta_{nj}^2}{2} = c_{nj} + d_{nj}\delta_{nj} \end{aligned} \tag{28}$$

Therefore:

$$\begin{aligned} u_n u_j \sin\delta_{nj} &\approx a'_{nj} + b'_{nj}\delta_{nj} + c'_{nj}u_n + d'_{nj}u_j \qquad (e.g.\ a'_{nj} = 2\mu_{u_n}\mu_{u_j}\mu_{\delta_{nj}}(-1 + \mu_{\delta_{nj}}^2/3)) \\ u_n u_j \cos\delta_{nj} &\approx a''_{nj} + b''_{nj}\delta_{nj} + c''_{nj}u_n + d''_{nj}u_j \end{aligned} \tag{29}$$

Taking into account equation (29) on equation (19), the following linearized equations are obtained:

$$\begin{aligned} p_{g,n} + p_{pv,n} - p_{l,n} - p_{wev,n} &= \sum_{j=1}^{N_n}\left(e'_{nj} + f'_{nj}\delta_n - f'_{nj}\delta_j + g'_{nj}u_n + h'_{nj}u_j\right) \\ q_{g,n} - q_{l,n} &= \sum_{j=1}^{N_n}\left(e''_{nj} + f''_{nj}\delta_n - f''_{nj}\delta_j + g''_{nj}u_n + h''_{nj}u_j\right) \end{aligned} \tag{30}$$

Coefficients e'_{nj}, e''_{nj}, f'_{nj}, f''_{nj}, g'_{nj}, g''_{nj}, h'_{nj}, and h''_{nj} are computed from RDS parameters and expected values of the output random variables in the RDS [61].

5.2.2. Cumulants method

The convolution of the random variables can be substituted by the summation of their cumulants, which greatly reduces the computational cost [62-64]. Thus, the cumulant method [40] (Figure 2) can be used to determine the cumulants of the output random variables in an RDS, i.e. nodal voltage angles and magnitudes by solving the linear system of equations (30), for each cumulant order of the input random variables, i.e. node loads, PV powers, and EV charging power.

5.2.3. Cornish-Fisher expansion

The Cornish-Fisher expansion [44] permits the reconstruction of the distribution function of a random variable from its cumulants (see Figure 2). The expansion is based on quantile estimation (inverse function of CDF).

6. SIMULATION RESULTS

The PPM was implemented in MATLAB and tested in the IEEE 33-node radial system (3,715 kW and 2,300 kVar [65]). The computer used in this research had a processor Intel(R) Core(TM)2 Duo CPU, 3 GHz, and 4 GB RAM. Although the results analyse the voltage profile of all the nodes of the test RDS, the voltage constraint fulfilment in node #18 (the most critical node for voltage regulation, Figure 3) and node #6 (internal RDS node with added EVs) was specifically verified.

6.1. Case studies

The main objective of the research was to assess the technical impact (voltage constraint fulfilment) within the context of PV and EV uncertainties on RDSs. According to regulations [35,36], four different scenarios without correlation were studied: (i) #1 base case (without EVs or PV); (ii) #2 (with EVs and without PV); (iii) #3 (without EVs and with PV); (iv) #4 (with EVs and PV). Furthermore, for the sake of completeness and because of space limitations, an additional scenario with correlation among input variables was evaluated: (i) #5 (scenario #4 with correlation). All scenarios were considered at the 10-min interval around noon (11:55-12:05) in January and July because of the very different PV impact in both months.

6.2. PV, node load, and EV data

The allocation of PV systems in the test RDS, according to [17,18], is shown in Figure 3. It consists of five PV systems with the same size and geographical location (see Table II), which add a peak PV power of 3.5 MWp. This represents a PV penetration about 15.06%[1], what is compatible with the penetration limit of the test RDS in [66].

Global irradiation data for the hourly diffuse fraction and the daily clearness index in the PV model were obtained from [67]. For correlated scenarios, the spatial PV dependence structure was modeled with a correlation matrix based on the spacing between nodes [68]. Thus, in the matrix correlation coefficients vary in the range of 0.95 to 0.65 from the closest to the furthest PV systems.

[1] PV capacity factor in the US ranges between 13% and 19% with an average of around 16%.

Table II. Characteristics of the PV system for each node.

Real and reactive load data in the test RDS nodes, were modelled as a normal distribution in each 10-min time-frame, are given in [17,18]. In particular, the time-conditional means (expected load values) for a 10-min interval were based on the case load in [65] and the specific daily modulation in [15]. Daily modulation around noon for January and July was 0.93 and 0.98 respectively. Furthermore, historical statistical data in [15] determined the standard deviation. Correlation coefficients for loads were set to 0.9 [23] for correlated scenarios.

There is a high level of uncertainty regarding how fast EV technology will penetrate the market. If penetration is moderate, the EPRI [69] states that by 2020, 30% of the total number of vehicles will be EVs. Thus, this research considers a mean EV penetration of 30%. Under this penetration, the resulting number of EVs to be considered in the test RDS was about 1,700 [7,9]. Mode #2 (Table I) was the one considered, since mode #1 was too slow, and mode #3 required a higher level of power. In addition, the connection of 1,700 EVs on few nodes, strategically distributed in the RDS, was assumed against a widespread connection of EVs to nodes. More specifically, three EV charging loads were connected to nodes #2, #6, and #14 (see Figure 3).

Regarding the main EV data, the annual mean and standard deviation of the daily distance driven by an EV was assumed to be equal to 36 and 9.4 km, respectively [7,9]. Based on survey information [7,8,11,12], the monthly means and standard deviations for the charging start time were in the interval 0:00-1:30 a.m. and 4.1-6.2 h, respectively.

Figure 3. Single-phase diagram of the IEEE 33-node radial system with PV systems and added EVs.

6.3. Results

6.3.1. PDF of the input random variables in the RDS

Meteorological, PV and EV data were used to calculate the moments, and then the cumulants of PV power and EV charging power in the selected RDS node for the 10-min interval around noon (11:55-12:05) in January and July (see Table III). The expected value of PV power, or first cumulant (κ_y^1), for both months significantly

differed due to the irradiation levels, whereas the means of the EV charging power were close. All results are given in p.u., and the power base and voltage base were chosen as 100 MVA and 12.66 kV, respectively.

Table III. Cumulants of PV power and charging power of all of the EVs in selected RDS nodes for the 10-min interval around noon.

Although all scenarios have been considered at the 10-min interval around noon, Figure 4 shows the PDFs of the PV power and EV charging power for two 10-min intervals in a day for comparison purposes. Obviously, as both powers were time-dependent, different 10-min intervals had different PDFs. The PDFs of the PV power did not follow any known distribution in January and July. In contrast, the PDF of the EV charging power fit a normal distribution. For this reason, there were only two cumulants, as shown in Table III.

Figure 4. PDFs of PV power and charging power of all of the EVs.

6.3.2. Comparison of concentrated connection of EVs on few nodes against a widespread connection

To justify the choice of a connection of EVs to three chosen nodes and not spread evenly over the RDS, the results of the 10-min voltage magnitude of node #6 at noon for both options are shown in Figure 5. As can be seen, the concentrated connection of EVs, i.e. the scenario #2, originated worse voltage values despite decreased dispersion. When more input variables were spread over the RDS (widespread connection), each one introduced a new uncertainty, which increased the dispersion of resulting PDFs.

Figure 5. PDF of the 10-min voltage magnitude at noon for node #6 in the defined scenarios.

6.3.3. Assessment of the technical impact of PV systems and EVs on RDSs

First, the assessment presents a general overview of the technical impact on the whole RDS. Thus, Table IV presents the results of the expected value and standard deviation of the 10-min voltage magnitude at noon for each RDS node in different scenarios. Figure 6 summarises the expected values for the previously defined scenarios.

Table IV. Expected value ($\mu_{\mathbf{u}^{1 \text{ or } 7}_{n,10\text{-}min_{11:55\text{-}12:05}}}$) and standard deviation ($\sigma_{\mathbf{u}^{1 \text{ or } 7}_{n,10\text{-}min_{11:55\text{-}12:05}}}$) of the 10-min voltage magnitude at noon for each RDS node in different scenarios.

Figure 6. Expected value of the 10-min voltage magnitude at noon for each RDS node in different scenarios.

Various conclusions can be derived from the results shown in Table IV and Figure 6. Initially, some voltage values in scenario #1 (base case) were closer to the -10% utilization voltage limit set forth by ANSI Std. C84.1 [36]. This revealed that actions would be performed in the RDS to improve certain voltages. This outcome was even more important if service voltage limits (range B) in ANSI Std. C84.1 [36] could be assumed, i.e. -5/5.8%.

When the EV charging loads were connected to the grid (scenario #2), the node voltages were even lower than in scenario #1. This caused an unacceptable condition for some nodes. Accordingly, the PV systems were connected to increase undesirable voltages. In both January and July, the voltage in problematic nodes (#10 to #18) increased noticeably. Nonetheless, in January, because of lower PV power (lower irradiation), there was less improvement. Anyway, the new voltage profile in nodes was smoother, and all voltages remained within standard limits.

As can be observed in Table IV, the standard deviation increased when more elements were connected to the grid. This was particularly evident in the PV or EV single condition (scenario #2 or #3) in comparison to when both elements were combined (scenario #4). This was because of the introduction of new variables in the RDS with an increased uncertainty, which originated a greater uncertainty in the output variables (i.e. node voltages). This effect was noticeably higher when the PV systems were connected because the standard deviation in output variables associated with PV power was much higher than that of the EV charging power.

Focusing on the voltage constraint fulfilment at specific nodes, Figures 7 and 8 show the resulting PDF and CDF of the PPM for the 10-min voltage magnitude at nodes #6 and #18, respectively. These figures highlight the higher dispersion associated with PV random power in relation to EV random charging power. Furthermore, the combined impact (#4) increased the dispersion of the output variable (i.e. the node voltage) even more. In addition, some PDFs departed from the Gaussian distribution because the PDFs of the PV random power were not Gaussian.

The correlation of input variables (#5) led to higher dispersions and expected values of voltage compared to those of the uncorrelated scenario (#4), increasing the probability of medium voltage levels.

Figure 7. PDF and CDF of the 10-min voltage magnitude at noon for node #6 in the defined scenarios.

Figure 8. PDF and CDF of the 10-min voltage magnitude at noon for node #18 in the defined scenarios.

The distribution function of voltage in each node (CDF or PDF) can be used to determine the probability of voltage threshold violation [70] set in service voltage limits by ANSI Std. C84.1 [36] (see Table V). Despite the fact that Table IV shows the mean voltage value at each RDS node, this value cannot be compared with the standard limit [36]. For example, the expected voltage value at node #6 in January (scenario #5) was 0.9508 p.u. (see Table IV) within standard limits. However, the relevant voltage violation probability was not 0 (see Table V). The voltage dispersion originated a voltage violation probability of 0.4968. In general, the probability study in Table V revealed a significant decrease in the voltage violation probability for the most of nodes when the combined impact of PV systems and EVs was considered in comparison to the single EV impact. This result emphasised how the PV systems in the test RDS with EVs noticeably helped to keep node voltages within regulation limits. Nonetheless, the higher dispersion of the resulting distributions under the combined effect still made the violation of voltage constraints probable.

Table V. Voltage violation probability, based on regulations, at noon for each RDS node in different scenarios.

6.3.4. Proposed probabilistic method (PPM) versus MCS

The reference method for assessing the accuracy of the analytical techniques is the mainstream MCS [18]. Particularly, the PPM includes three error sources compared to the MCS. These error sources are the following: (i) the use of a higher or lower number of cumulants to characterize the input variables, i.e., more orders of cumulants or fewer; (ii) the application of the linear approximation of the non-linear load-flow equations; (iii) the use of a shorter or longer Cornish-Fisher expansion with more cumulants or fewer.

Although more cumulants produce better results in point (i) and (iii), practically speaking, numerical cumulants higher than the fifth-order are not required for the proposed analytical technique which is based on the Cornish-Fisher expansion [18,41,71,72]. Nonetheless, other expansions, such as Gram-Charlier expansion, could require up to 7 cumulants [63]. Therefore, in our study, the fifth order should really be the significant upper limit for comparison purposes.

The PPM and MCS can only be compared on the basis of their results. The accuracy assessment of our PPM, compared with MCS, took into account the three previously mentioned error sources. This accuracy of the PPM was carried out by means of the individual relative error of the first seven moments for each RDS output variable. In particular, this error in the voltage magnitude at any *n*th node, *x*th10-min interval of the day (t_x), and *m*th month is given by [73]:

$$\varepsilon_{\alpha^{1...1}_{\mathbf{u}^m_{n,10\text{-}min_{t_x}}}} = \frac{100 \cdot \left| \alpha^{r}_{\mathbf{u}^m_{n,10\text{-}min_{t_x}}}(1...1, \mathbf{PPM}) - \alpha^{r}_{\mathbf{u}^m_{n,10\text{-}min_{t_x}}}(1...1, \mathbf{MCS}) \right|}{\alpha^{r}_{\mathbf{u}^m_{n,10\text{-}min_{t_x}}}(1...1, \mathbf{MCS})} \tag{31}$$

Table VI shows that the expected values and standard deviations (first two moments) could be accurately estimated using the PPM for the most critical node (node #18) and under the assumption of several scenarios; the maximum error (0.087% for mean value and 1.83% for standard deviation) was achieved in scenario #4. This is consistent regarding the error associated with the power flow linearization; when more input variables were spread over the RDS (scenario #4 vs. #2 or #3), each one introduced a new dispersion in the input variable decreasing slightly the accuracy of the linear approximation.

The higher moments until fifth order were nearly accurate. Thus, maximum error is capped at a level of 3.74%. This error level was much smaller than relevant errors shown in similar works under analytical techniques (e.g. 45.26% [18], 72.47% [41], 3.88% [71], 59.36% [72]). In other words, the PPM had similar accuracy levels to the MCS for calculating the statistics of voltage magnitude. The higher moments, not really relevant in the PPM, showed up to 6.12% of difference.

Table VII illustrates that computation time needed by PPM was much less than MCS, but achieving the same accuracy.

Table VI. Individual relative error of the first seven moments of the 18-node voltage magnitude.

Table VII. Run time comparison.

7. CONCLUSIONS

This paper has analysed the fulfilment of voltage constraints in a test RDS under the single or combined impact of PV systems and EVs. This study was carried out from a probabilistic perspective that took into account the uncertainty. This uncertainty was associated with the previously mentioned generation and consumption powers. Therefore, it was first necessary to model the PV systems and EV charging loads as random variables. In order to verify the voltage constraint fulfilment in regulations [35,36], the PPM in this study combined the calculation of input variable cumulants, the linearization of load flow equations, the cumulant method, and the Cornish-Fisher expansion.

The MCS was used in order to highlight the accuracy of the results of our method. Moreover, it achieved a high computational cost reduction in comparison to the MCS.

The results has demonstrated that the voltage violation probability in the nodes of the IEEE 33-node RDS with EV charging loads decreased significantly when PV systems were connected to the RDS. Nonetheless, the introduction of new random variables in the RDS (PV systems), with an increased uncertainty, originated a greater dispersion in the resulting distributions of the output variables. Consequently, in spite of a lower voltage violation probability, the voltage constraint fulfilment in regulations could not be absolutely guaranteed. In addition, the results indicated that the correlation among input variables had major impact on the node voltage. This new approach gave us a more accurate assessment than other evaluations, based on a simple deterministic vision. This PPM thus enhances the planning and operation of RDSs and offers a better understanding of the combined technical impact.

In the future, this tool can act as a bridge between PV and EV uncertainties and deterministic approaches for the analysis of RDSs. It is valuable because it provides crucial information for designers of RDSs with EVs and PV systems. Therefore, coming research may include the PPM in an optimization process to determine the location and size of the PV systems and EVs in RDSs.

8. ACKNOWLEDGEMENTS

This research was funded by the Spanish Ministry of Economy and Competitiveness under Grant ENE2015-46205-C5-1-R.

9. LIST OF SYMBOLS AND ABBREVIATIONS

a_i	real constants
CDF	cumulative distribution function
COP	Copula
$\boldsymbol{d}$ [1]	daily distance driven by an EV, km
d_r	maximum range of an EV, km
$\boldsymbol{E}$	initial SOC of the EV battery at the beginning of a recharge cycle, %
E	discrete SOC of the EV battery, %
EV	electric vehicle
EV	electric vehicle
f	number of lines in the RDS
$f^*_{X_i}(\boldsymbol{X_i})$	PMF of the discrete univariate random variable $\boldsymbol{X_i}$
$F_{X_i}(\boldsymbol{X_i})$	CDF of the univariate random variable $\boldsymbol{X_i}$
$F^{-1}_{X_i}$	inverse distribution function of the univariate random variable $\boldsymbol{X_i}$
$g_{nj}(b_{nj})$	series conductance (susceptance) of branch node *n* to node *j*, pu
$h_{t_k}(\boldsymbol{t_k})$	PDF of the random variable charging start time of the EV battery
i	nodal current injection, pu
j^{L_f}	current in branch L_f, pu
$\boldsymbol{k_d}$	hourly diffuse fraction, pu
$\boldsymbol{K_T}$	daily clearness index, pu
m	any given month (m = 1,…,12)
MCS	Monte Carlo simulation
n_s	correlated random input samples
n	any given RDS node
N_c	number of 10-min intervals required for a full charging process of the EV battery
N_{ev}	number of RDS nodes with EV
N_l	number of RDS nodes with loads
N_n	nodes number of the RDS
N_{pv}	number of RDS nodes with PV systems
N_{rv}	random variable number
$p(q)$	real(reactive) power injection, pu
$\boldsymbol{p_{ev}}(\boldsymbol{p_{wev}})$	charging power of an EV (the whole EVs in a node), pu

[1] Bold letters are used to random variables

p_{ev}	discrete charging power level of the EV battery, pu
$p_{ev}^{\Diamond}$	continuous charging power of the EV battery, pu
$p_g(q_g)$	real(reactive) generation power of a traditional generator, pu
$\boldsymbol{p}_l(\boldsymbol{q}_l)$	active (reactive) load power, pu
$\boldsymbol{p}_{pv}$	PV power, pu
PDF	probability density function
PMF	probability mass function
PPM	proposed probabilistic method
PV	photovoltaic
RDS	radial distribution system
s	apparent power injection, pu
SOC	state-of-charge
t_1 , t_2	times that determine the variation in the charging power magnitude, min
$\boldsymbol{t_k}$	charging start time of the EV battery, min
t_x	xth 10-min interval
T	step time for the discretization of charging profile of an EV battery (10-min interval), min
u	node voltage, pu
$\boldsymbol{U}_i(\boldsymbol{U}_{\boldsymbol{X}_i})$	univariate uniform distribution (associated with random variable $\boldsymbol{X}_i$)
$\boldsymbol{W}_{\boldsymbol{X}_i}$	univariate standard normal distribution associated with random variable $\boldsymbol{X}_i$
x	any given number
$\boldsymbol{X}$	multivariable random variable $(=[\boldsymbol{X}_1, \boldsymbol{X}_2, ..., \boldsymbol{X}_{N_{rv}}]^{\mathrm{T}})$
y_n	sum of all the shunt elements at the node n, pu
z^{L_f}	series impedance of branch L_f, pu
Greek symbols	
$\alpha_{\boldsymbol{X}}^{i_1 \ldots i_r}$ $(\kappa_{\boldsymbol{X}}^{i_1 \ldots i_r})$	rth-order moment (cumulant) of the random variable $\boldsymbol{X}$
$\alpha^{1 \ldots 1,\ \mathbf{PPM}}_{\boldsymbol{u}^m_{n,10\text{-}min_{t_x}}}$	rth-order moment of the RDS output variable $\boldsymbol{u}^m_{n,10\text{-}min_{t_x}}$ obtained by PPM
$(\alpha^{1 \ldots 1,\ \mathbf{MCS}}_{\boldsymbol{u}^m_{n,10\text{-}min_{t_x}}})$	(MCS)
$\varepsilon_{\alpha^{1 \ldots 1}_{\boldsymbol{u}^m_{n,10\text{-}min_{t_x}}}}$	individual relative error of rth-order moment of the RDS output variable $\boldsymbol{u}^m_{n,10\text{-}min_{t_x}}$
λ	number of EVs in a given set
$\mu_{X_i}(\sigma_{X_i})$	expected value (standard deviation) of the random variable $\boldsymbol{X}_i$
ρ_{X_i, X_j}	ijth correlation coefficient in matrix $\sum_{\boldsymbol{X}}$
$\sum_{\boldsymbol{X}}$	correlation matrix of multivariate random variable $\boldsymbol{X}$
φ	singleton probability
ϕ	CDF of the univariate standard normal distribution
ϕ^{-1}	inverse of the univariate standard normal distribution

δ_{in}	phase angle of voltage from node *i* to node *n*, pu

Subscripts

ev	electric vehicle
l	load
n	*n*th node of the RDS
pv	photovoltaic
$10\text{-}min_j$	*j*th 10-min interval
$10\text{-}min_{t_x}$	*x*th10-min interval (t_x)

Superscripts

(*k*)	at *k*th iteration
m	*m*th month
L_f	L_f th line of the RDS

REFERENCES

1. Alley R et al. Climate change 2007: the physical science basis, summary for policymakers. Intergovernmental Panel on Climate Change. 2007.
2. International Energy Agency. [Online]. Available: http://www.iea.org, accessed January 2017.
3. The WorldWatch Institute. The world state of the world. Innovations for a sustainable economy. [Online]. Available: http://www.worldwatch.org, accessed accessed January 2017.
4. EurObserv'ER. Baromètre Photovoltaïque: Systèmes Solaires. Le journal des énergies renouvelables. [Online]. Available: http://www.energies-renouvelables.org, accessed January 2017.
5. Rezaee S, Farjah E, Khorramdel B. Probabilistic analysis of plug-in electric vehicles impact on electrical grid through homes and parking lots. *IEEE Transactions on Sustainable Energy* 2013; **4**:1024–1033. DOI: 10.1109/TSTE.2013.2264498.
6. Sexauer JM, McBee KD, Bloch KA. Applications of probability model to analyze the effects of electric vehicle chargers on distribution transformers. *IEEE Transactions on Power Systems* 2013; **28**:847–854. DOI: 10.1109/EPEC.2011.6070213.
7. ElNozahy MS, Salama MMA. A comprehensive study of the impacts of PHEVS on residential distribution networks. *IEEE Transactions on Sustainable Energy* 2014; **5**:332–342. DOI: 10.1109/PESGM.2014.6939045.
8. Leemput N, Geth F, Van Roy J, et al. Impact of electric vehicle on-board single-phase charging strategies on a Flemish residential grid. *IEEE Transactions on Smart Grid* 2014; **5**:1815–1822. DOI: 10.1109/TSG.2014.2307897.
9. Leou R-C, Su C-L, Lu C-N. Stochastic analyses of electric vehicle charging impacts on distribution network. *IEEE Transactions on Power Systems* 2014; **29**:1055–1063. DOI: 10.1109/TPWRS.2013.2291556.
10. Khorramdel B, Khorramdel H, Aghaei J, et al. Voltage security considerations in optimal operation of BEVS/PHEVS integrated microgrids. *IEEE Transactions on Smart Grid* 2015; **6**:1575–1587. DOI: 10.1109/TSG.2015.2394499.
11. Qian K, Zhou C, Allan M, Yuan Y. Modeling of load demand due to EV battery charging in distribution systems. *IEEE Transactions on Power Systems* 2011; **26**:802–810. DOI: 10.1109/TPWRS.2010.2057456.
12. Zhang P, Qian K, Zhou C, Stewart BG, Hepburn DM. A methodology for optimization of power systems demand due to EV charging load. *IEEE Transactions on Power Systems* 2012; **27**:1628–1636. DOI: 10.1109/TPWRS.2012.2186595.
13. Nafisi H, Abyaneh HA, Abedi M. Energy loss minimization using PHEVs as distributed active and reactive power resources: a convex quadratic local optimal solution. *International Transactions on Electrical Energy Systems* 2016; **26**:1287–1302. DOI: 10.1002/etep.2134.
14. Hernandez JC, Medina A, Jurado F. Optimal allocation and sizing for profitability and voltage enhancement of PV systems on feeders. *Renewable Energy* 2007; **32**:1768–1789. DOI: 10.1016/j.renene.2006.11.003.

15. Hernandez JC, Medina A, Jurado F. Impact comparison of PV system integration into rural and urban feeders. *Energy Conversion and Management* 2008; **49**:1747–1765. DOI: 10.1016/j.enconman.2007.10.020.
16. Marinopoulos AG, Alexiadis MC, Dokopoulos PS. Energy losses in a distribution line with distributed generation based on stochastic power flow. *Electric Power Systems Research* 2011; **81**:1986–1994. DOI: 10.1016/j.epsr.2011.06.006.
17. Ruiz-Rodriguez FJ, Hernandez JC, Jurado F. Probabilistic load flow for radial distribution networks with photovoltaic generators. *IET Renewable Power Generation* 2012; **6**:110–121. DOI: 10.1049/iet-rpg.2010.0180.
18. Ruiz-Rodriguez FJ, Hernandez JC, Jurado F. Probabilistic load flow for photovoltaic distributed generation using the Cornish–Fisher expansion. *Electric Power Systems Research* 2012; **89**:129–138. DOI: 10.1016/j.epsr.2012.03.009.
19. Caramia P, Garpinelli G, Varilone P. Point estimate schemes for probabilistic three-phase load flow. *Electric Power Systems Research* 2010; **80**:168–75. DOI: 10.1016/j.epsr.2009.08.020.
20. Nikmehr N, Ravadanegh SN. A study on optimal power sharing in interconnected microgrids under uncertainty. *International Transactions on Electrical Energy Systems* 2016; **26**:208–232. DOI: 10.1002/etep.2081.
21. Maya KN, Jasmin EA. Optimal integration of distributed generation (DG) resources in unbalanced distribution system considering uncertainty modelling. *International Transactions on Electrical Energy Systems* 2016; DOI: 10.1002/etep.2248.
22. Lei X, Yan W-J, Peng P, Ye T. An optimal purchase and sale power model considering microgrids. *International Transactions on Electrical Energy Systems* 2015; **25:**246–261. DOI: 10.1002/etep.1839.
23. Li X, Zhang X, Wu L. Lu P, Zhang S. Transmission line overload risk assessment for power systems with wind and load-power generation correlation. *IEEE Transactions on Smart Grid* 2015; **6**: 1233–1242. DOI: 10.1109/TSG.2014.2387281.
24. Munkhammar J, Widén J, Rydén J. On a probability distribution model combining household power consumption, electric vehicle home-charging and photovoltaic power production. *Applied Energy* 2015; **142**: 135–143. DOI: 10.1016/j.apenergy.2014.12.031.
25. Carrión M, Zárate-Miñano R. Operation of renewable-dominated power systems with a significant penetration of plug-in electric vehicles. *Energy* 2015; **90**: 827–835. DOI: 10.1016/j.energy.2015.07.111.
26. ElNozahy MS, Abdel-Galil TK, Salama MMA. Probabilistic ESS sizing and scheduling for improved integration of PHEVs and PV systems in residential distribution systems. *Electric Power Systems Research* 2015; **125**: 55-66. DOI: 10.1016/j.epsr.2015.03.029.
27. Tovilović DM, Rajaković NLJ. The simultaneous impact of photovoltaic systems and plug-in electric vehicles on the daily load and voltage profiles and the harmonic voltage distortions in urban distribution systems. *Renewable Energy* 2015; **76**: 454–464. DOI: 10.1016/j.renene.2014.11.065
28. Wu C, Wen F, Lou Y, Xin F. Probabilistic load flow analysis of photovoltaic generation system with plug-in electric vehicles. *International Journal of Electrical Power & Energy Systems* 2015; **64**: 1221–1228. DOI: 10.1016/j.ijepes.2014.09.014.
29. Hung DQ, Dong ZY, Trinh H. Determining the size of PHEV charging stations powered by commercial grid-integrated PV systems considering reactive power support. *Applied Energy* 2016; **183**:160–169. DOI: 10.1016/j.apenergy.2016.08.168.
30. Kabir MN, Mishra Y, Bansal RC. Probabilistic load flow for distribution systems with uncertain PV generation. *Applied Energy* 2016; **163**: 343**–**351. DOI: 10.1016/j.apenergy.2015.11.003.
31. Gray MK, Morsi WG. On the impact of single-phase plug-in electric vehicles charging and rooftop solar photovoltaic on distribution transformer aging. *Electric Power Systems Research* 2017; **148**: 202–209. DOI: 10.1016/j.epsr.2017.03.022.
32. Tabatabaee S, Mortazavi SS, Niknam T. Stochastic scheduling of local distribution systems considering high penetration of plug-in electric vehicles and renewable energy sources. *Energy* 2017; **121**: 480–490. DOI: 10.1016/j.energy.2016.12.115.
33. Hernandez JC, De la Cruz J, Ogayar B. Electrical protection for the grid-interconnection of photovoltaic-distributed generation. *Electric Power Systems Research* 2012; **89**:85–99. DOI: 10.1016/j.epsr.2012.03.002.
34. Sanchez-Sutil F, Hernandez JC, Tobajas C. Overview of electrical protection requirements for integration of a smart DC node with bidirectional electric vehicle charging stations into existing AC and DC railway grids. *Electric Power Systems Research* 2015; **122**:104–118. DOI: 10.1016/j.epsr.2015.01.003.

35. IEEE Standard 1547. Standard for interconnecting distributed resources with electric power systems, 2003.
36. ANSI Standard C84.1. American national standard for electric power systems and equipment-Voltage ratings (60 Hertz), 2011.
37. EN Standard 50160. Voltage characteristics of electricity supplied by public distribution systems, 2000.
38. Borkowska B. Probabilistic load flow. *IEEE Transactions on Power Apparatus and Systems* 1974; **93**:752–755.
39. Rubinstein RY. Simulation and the Monte Carlo method. John Wiley and Sons; 1989.
40. McCullagh P. Tensor methods in statistics. London: Chapman and Hall; 1987.
41. Usaola J. Probabilistic load flow with correlated wind power injections. *Electric Power Systems Research* 2010; **80**: 528–536. DOI: 10.1016/j.epsr.2009.10.023.
42. Kendall MG, Stuart A. The advanced theory of statistics. Vol. I. London: Charles Grin and Company Limited; 1963.
43. Ruiz-Rodriguez FJ, Jurado F. Modeling of photovoltaic generator as a random variable. Gill MA, Nova Science Publishers; 2014; 91–119.
44. Cornish EA, Fisher RA. Moments and cumulants in the specification of distributions. *Revue de l'Institut International de Statis* 1937; **5**:307–322.
45. Jardini JA, Tahan CMV, Gouvea MR, Ahn SU, Figueiredo FM. Daily load profiles for residential, commercial industrial low voltage consumers. *IEEE Transactions on Power Delivery 2000*; **15**:375–380. DOI: 10.1109/61.847276.
46. Espinoza M, Belmans CJR, Moor BD. Short-term load forecasting, profile identification, and customer segmentation: a methodology based on periodic time series. *IEEE Transactions on Power Systems* 2005; **20**:1622–1630. DOI: 10.1109/TPWRS.2005.852123.
47. Caramanis MC, Tabors RD, Nochur KS, Schweppe FC. The introduction of non-dispatchable technologies as decision variables in long-term generation expansion models. *IEEE Transactions on Power Apparatus & System* 1982; **PAS-101**: 2658–2666. DOI: 10.1109/MPER.1982.5519756.
48. Madrid C, Argueta J, Smith J. Performance characterization-1999 Nissan Altra-EV with lithium-ion battery. Southern California EDISON; 1999.
49. IEC Standard 61851-1. Electric vehicle conductive charging system - General requirements, 2010.
50. Ochoa LF, Dent CJ, Harrison GP. Distribution network capacity assessment: Variable DG and active networks. *IEEE Transactions on Power Systems* 2010; **25**: 87–95. DOI: 10.1109/TPWRS.2009.2031223.
51. Verbic G, Cañizares CA. Probabilistic optimal power flow in electricity markets based on a two-point estimate method. *IEEE Transactions on Power Systems 2006*; **21**: 1883–1893. DOI: 10.1109/TPWRS.2006.881146.
52. Bright JM, Babacan O, Kleiss J, Taylor PG, RCrook. A synthetic, spatially decorrelating solar irradiance generator and application to a LV grid model with high PV penetration. *Solar Energy* 2017; **147**: 83–98. DOI: 10.1016/j.solener.2017.03.018.
53. Papaefthymiou G, Kurowicka D. Using copulas for modeling stochastic dependence in power system uncertainty analysis. *IEEE Transactions on Power Systems* 2009; **24**: 40–49. DOI: 10.1109/TPWRS.2008.2004728.
54. Kurowicka D, Cooke RM. Uncertainty analysis with high dimensional dependence modelling. New York: Wiley; 2006.
55. Liu P-L, Kiureghian A. Multivariate distribution models with prescribed marginals and covariances. *Probabilistic Engineering Mechanics* 1986; **1**: 101–112. DOI: 10.1016/0266-8920(86)90033-0.
56. Qin Z, Li W, Xiong X. Generation system reliability evaluation incorporating correlations of wind speeds with different distributions. *IEEE Transactions on Power Systems* 2013; **28**: 551–558. DOI: 10.1109/TPWRS.2012.2205410.
57. Cario M, Nelson B. Modeling and generating random vectors with arbitrary marginal distribution and correlation matrix. Northwestern University, Evanston, IL, USA, Apr. 1997, Tech. Rep.
58. Madsena L, Birkes D. Simulating dependent discrete data. *Journal of Statistical Computation Simulation* 2011; **1**: 677–691.
59. Morales JM, Conejo AJ, Perez-Ruiz J. Simulating the impact of wind production on locational marginal prices. *IEEE Transactions on Power Systems* 2011; **26**: 820–828. DOI: 10.1109/TPWRS.2010.2052374.
60. Shirmohammamdi D, Hong HW, Semlyen A, Luo GX. A compensation-based power flow method for weakly Meshed distribution and transmission network. *IEEE Transactions on Power Systems* 1988; **3**:753–762. DOI: 10.1109/59.192932.

61. Anders J. Probability concepts in electric power systems. New York: John Wiley and Sons; 1990.
62. Anders GJ. Probability concepts in electric power systems. New York: John Wiley and Sons; 1990.
63. Zhang P, Lee ST. Probabilistic load flow computation using the method of combined cumulants and Gram-Charlier expansion. *IEEE Transactions on Power Systems* 2004; **19**:676–682. DOI: 10.1109/TPWRS.2003.818743.
64. Sanabria IA, Dillon TS. An error correction algorithm for stochastic production costing. *IEEE Transactions on Power Systems* 1988; **3**:94–100. DOI: 10.1109/59.43185.
65. Baran ME, Wu FF. Network reconfiguration in distribution systems for loss reduction and load balancing. *IEEE Transactions on Power Delivery* 1989; **4**: 1401–1407. DOI: 10.1109/61.25627.
66. Hung DQ, Mithulananthan N, Lee KY. Determining PV penetration for distribution systems with time-varying load models. *IEEE Transactions on Power Systems* 2014; **29**; 3048–3057. DOI: 10.1109/TPWRS.2014.2314133.
67. National Solar Radiation Data Base. National Renewable Energy Laboratoy. Available [Online]: http://rredc.nrel.gov/solar/old_data/nsrdb/ [Accessed May 2017].
68. Hernandez JC, Ruiz-Rodriguez FJ, Jurado F. Technical impact of photovoltaic-distributed generation on radial distribution systems: Stochastic simulations for a feeder in Spain. *International Journal of Electrical Power & Energy Systems* 2013; **50:** 25-32. DOI: 10.1016/j.ijepes.2013.02.010.
69. Environmental assessment of plug-in hybrid electric vehicles, nationwide greenhouse gas emissions. Tech. Rep. 1015325 EPRI and NRDC 1 (2007) 1–56.
70. Ruiz-Rodriguez FJ, Gomez-Gonzalez M, Jurado F. A method for reliability optimization of distributed generation using meta-heuristic and probabilistic techniques. *Electric Power Components and Systems* 2015; **43**: 32–43. DOI: 10.1080/15325008.2014.963262.
71. Usaola J. Probabilistic load flow with wind production uncertainty using cumulants and Cornish-Fisher expansion. *International Journal of Electrical Power & Energy Systems* 2009; **31**: 474–481. DOI: 10.1016/j.ijepes.2009.02.003.
72. Usaola J. Probabilistic load flow in systems with wind generation. *IET Generation, Transmission, and Distribution* 2009; **3**: 1031–1041. DOI: 10.1049/iet-gtd.2009.0039.
73. Huang H, Chung CY, Chan KW, Chen H. Quasi-Monte Carlo based probabilistic small signal stability analysis for power systems with plug-in electric vehicle and wind power integration. *IEEE Transactions on Power Systems* 2013; **28**: 3335–3343. DOI: 10.1109/TPWRS.2013.2254505.

LIST OF TABLES AND FIGURES

Table I. Parameters of EV battery charging profile.

Mode	#1	#2	#3 and #4
Power (P_{ev})	3.5 kW	6.6 kW	40 kW
t_1 [a]	6.3 h	3.6 h	0.50 h
t_2 [a]	8 h	4 h	0.75 h
N_c	48	24	5 [b]

[a] Times according to Figure 1; [b] Rounded upwards because charging time is a decimal

Table II. Characteristics of the PV system for each node.

	Winter	Summer
Latitude, º	40	40
Time (noon), h	11:55-12:05	11:55-12:05
Month	January	July
Day of the year	15	185
Inclination panel, º	40	30
Peak PV power, kWp	700	700

Table III. Cumulants of PV power and charging power of all of the EVs in selected RDS nodes for the 10-min interval around noon.

Cumulants	PV power ($y = p^{1 \text{ or } 7}_{pv,n,10\text{-}min_{11:55\text{-}12:05}}$, n=12, 17, 21, 24, 32)		EV charging power ($y = p^{1 \text{ or } 7}_{wev,n,10\text{-}min_{11:55\text{-}12:05}}$, n=3, 6, 14)	
	January	July	January	July
κ_y^1	0.002295	0.0054	0.00396	0.00354
κ_y^{11}	6.5915e-06	1.1944e-06	3.7516-08	3.8366e-08
κ_y^{111}	-1.4351e-08	-1.6496e-09	0.0	0.0
κ_y^{1111}	1.2022e-11	2.7362e-12	0.0	0.0
κ_y^{11111}	1.5060e-13	-3.2629e-15	0.0	0.0
κ_y^{111111}	-1.1334e-15	-8.4059e-18	0.0	0.0
$\kappa_y^{1111111}$	1.5059e-18	9.8968e-20	0.0	0.0

Table IV. Expected value ($\mu_{\mathbf{u}^{1\text{ or }7}_{n,10\text{-}min_{11:55\text{-}12:05}}}$) and standard deviation ($\sigma_{\mathbf{u}^{1\text{ or }7}_{n,10\text{-}min_{11:55\text{-}12:05}}}$) of the 10-min voltage magnitude at noon for each RDS node in different scenarios.

Month Scenario	January #1 (base case)		January #2 (with EVs, without PV)		July #2 (with EVs, without PV)		January #4 (with EVs, with PV)		July #4 (with EVs with PV)		January #5 (with EVs, with PV)		July #5 (with EVs with PV)	
Node	$\mu_{\mathbf{u}^1_{n,10\text{-}min_{11:55\text{-}12:05}}}$	$\sigma_{\mathbf{u}^1_{n,10\text{-}min_{11:55\text{-}12:05}}}$	$\mu_{\mathbf{u}^1_{n,10\text{-}min_{11:55\text{-}12:05}}}$	$\sigma_{\mathbf{u}^1_{n,10\text{-}min_{11:55\text{-}12:05}}}$	$\mu_{\mathbf{u}^7_{n,10\text{-}min_{11:55\text{-}12:05}}}$	$\sigma_{\mathbf{u}^7_{n,10\text{-}min_{11:55\text{-}12:05}}}$	$\mu_{\mathbf{u}^1_{n,10\text{-}min_{11:55\text{-}12:05}}}$	$\sigma_{\mathbf{u}^1_{n,10\text{-}min_{11:55\text{-}12:05}}}$	$\mu_{\mathbf{u}^7_{n,10\text{-}min_{11:55\text{-}12:05}}}$	$\sigma_{\mathbf{u}^7_{n,10\text{-}min_{11:55\text{-}12:05}}}$	$\mu_{\mathbf{u}^1_{n,10\text{-}min_{11:55\text{-}12:05}}}$	$\sigma_{\mathbf{u}^1_{n,10\text{-}min_{11:55\text{-}12:05}}}$	$\mu_{\mathbf{u}^7_{n,10\text{-}min_{11:55\text{-}12:05}}}$	$\sigma_{\mathbf{u}^7_{n,10\text{-}min_{11:55\text{-}12:05}}}$
	(p.u.)		(p.u.)		(p.u.)		(p.u.)		(p.u.)		(p.u.)		(p.u.)	
#2	0.9970	3.8e-5	0.9960	3.2e-5	0.9963	3.2e-05	0.9970	0.0005	0.9980	0.0008	0.9990	0.0005	0.9999	0.0010
#3	0.9829	0.0002	0.9792	0.0002	0.9796	0.0002	0.9833	0.0028	0.9885	0.0035	0.9853	0.0031	0.9905	0.0046
#4	0.9754	0.0003	0.9695	0.0003	0.9702	0.0003	0.9756	0.0042	0.9831	0.0051	0.9775	0.0047	0.9851	0.0071
#5	0.9679	0.0004	0.9598	0.0003	0.9608	0.0003	0.9679	0.0057	0.9780	0.0070	0.9698	0.0063	0.9799	0.0097
#6	*0.9485*	*0.0007*	*0.9319*	*0.0006*	*0.9341*	*0.0005*	*0.9489*	*0.0091*	*0.9601*	*0.0109*	*0.9508*	*0.0103*	*0.9664*	*0.0147*
#7	0.9460	0.0007	0.9298	0.0006	0.9290	0.0005	0.9455	0.0097	0.9619	0.0117	0.9474	0.0109	0.9638	0.0163
#8	0.9323	0.0009	0.9131	0.0006	0.9154	0.0006	0.9325	0.0149	0.9563	0.0175	0.9344	0.0167	0.9582	0.0239
#9	0.9260	0.0010	0.9036	0.0006	0.9063	0.0006	0.9266	0.0180	0.9548	0.0214	0.9285	0.0203	0.9567	0.0294
#10	0.9201	0.0011	0.8945	0.0006	0.8976	0.0006	0.9212	0.0213	0.9538	0.0252	0.9230	0.0239	0.9557	0.0345
#11	0.9192	0.0011	0.8931	0.0006	0.8962	0.0005	0.9204	0.0219	0.9539	0.0260	0.9222	0.0247	0.9558	0.0355
#12	0.9177	0.0012	0.8905	0.0006	0.8938	0.0005	0.9190	0.0231	0.9541	0.0272	0.9208	0.0259	0.9560	0.0376
#13	0.9115	0.0013	0.8799	0.0004	0.8837	0.0004	0.9112	0.0257	0.9495	0.0303	0.9129	0.0289	0.9514	0.0417
#14	0.9092	0.0014	0.8760	0.0004	0.8800	0.0003	0.9082	0.0267	0.9478	0.0315	0.9101	0.0301	0.9497	0.0432
#15	0.9078	0.0014	0.8745	0.0005	0.8785	0.0004	0.9077	0.0278	0.9485	0.0327	0.9096	0.0313	0.9504	0.0447
#16	0.9064	0.0014	0.8730	0.0005	0.8771	0.0005	0.9076	0.0291	0.9499	0.0346	0.9094	0.0328	0.9518	0.0472
#17	0.9044	0.0014	0.8709	0.0006	0.8750	0.0006	0.9075	0.0315	0.9525	0.0373	0.9094	0.0355	0.9544	0.0513
#18	*0.9038*	*0.0015*	*0.8703*	*0.0007*	*0.8783*	*0.0006*	*0.9069*	*0.0316*	*0.9419*	*0.0373*	*0.9087*	*0.0303*	*0.9537*	*0.0518*
#19	0.9965	4.3e-5	0.9957	3.8e-5	0.9958	3.8e-05	0.9967	0.0006	0.9980	0.0008	0.9987	0.0007	0.9999	0.0010
#20	0.9929	0.0001	0.9921	0.0001	0.9922	0.0001	0.9953	0.0037	0.9995	0.0047	0.9973	0.0042	1.0000	0.0066
#21	0.9922	0.0002	0.9914	0.0002	0.9915	0.0001	0.9952	0.0044	1.0001	0.0058	0.9972	0.0050	1.0007	0.0081
#22	0.9916	0.0002	0.9908	0.0002	0.9908	0.0002	0.9946	0.0044	0.9996	0.0058	0.9966	0.0050	1.0000	0.0081
#23	0.9793	0.0003	0.9756	0.0003	0.9760	0.0003	0.9804	0.0033	0.9865	0.0043	0.9824	0.0036	0.9884	0.0061
#24	0.9726	0.0006	0.9689	0.0005	0.9693	0.0005	0.9751	0.0048	0.9830	0.0062	0.9770	0.0053	0.9849	0.0086
#25	0.9693	0.0007	0.9655	0.0007	0.9660	0.0006	0.9717	0.0048	0.9797	0.0066	0.9737	0.0053	0.9816	0.0091
#26	0.9476	0.0007	0.9344	0.0006	0.9360	0.0006	0.9473	0.0093	0.9633	0.0113	0.9492	0.0104	0.9652	0.0157
#27	0.9450	0.0008	0.9318	0.0007	0.9334	0.0006	0.9452	0.0097	0.9618	0.0117	0.9471	0.0109	0.9637	0.0163
#28	0.9335	0.0010	0.9202	0.0010	0.9218	0.0009	0.9354	0.0115	0.9544	0.0144	0.9373	0.0129	0.9563	0.0198
#29	0.9253	0.0012	0.9118	0.0012	0.9135	0.0011	0.9285	0.0129	0.9493	0.0163	0.9303	0.0146	0.9512	0.0224
#30	0.9218	0.0013	0.9082	0.0013	0.9098	0.0012	0.9258	0.0139	0.9476	0.0175	0.9276	0.0157	0.9495	0.0239
#31	0.9176	0.0014	0.9040	0.0014	0.9056	0.0013	0.9231	0.0158	0.9470	0.0198	0.9249	0.0177	0.9489	0.0274
#32	0.9167	0.0014	0.9031	0.0014	0.9047	0.0013	0.9227	0.0164	0.9473	0.0206	0.9246	0.0185	0.9492	0.0279
#33	0.9164	0.0014	0.9028	0.0014	0.9044	0.0013	0.9224	0.0164	0.9470	0.0206	0.9243	0.0185	0.9489	0.0279

Table V. Voltage violation probability, based on regulations, at noon for each RDS node in different scenarios.

Month Scenario	January #2 (with EVs, without PV)	July #2 (with EVs, without PV)	January #5 (with EVs, with PV)	July #5 (with EVs, with PV)	Month Scenario	January #2 (with EVs, without PV)	July #2 (with EVs, without PV)	January #5 (with EVs, with PV)	July #5 (with EVs, with PV)
#2	0.0000	0.0000	0.0000	0.0000	*#18*	*1.0000*	*1.0000*	0.8318	0.5044
#3	0.0000	0.0000	0.0000	0.0000	#19	0.0000	0.0000	0.0000	0.0000
#4	0.0000	0.0000	0.0000	0.0000	#20	0.0000	0.0000	0.0000	0.0000
#5	0.0000	0.0000	0.0976	0.0867	#21	0.0000	0.0000	0.0000	0.0000
#6	*1.0000*	*1.0000*	0.4968	0.4153	#22	0.0000	0.0000	0.0000	0.0000
#7	1.0000	1.0000	0.5240	0.4251	#23	0.0000	0.0000	0.0000	0.0000
#8	1.0000	1.0000	0.5891	0.4658	#24	0.0000	0.0000	0.0000	0.0009
#9	1.0000	1.0000	0.6125	0.4689	#25	0.0000	0.0000	0.0076	0.0026
#10	1.0000	1.0000	0.6578	0.4710	#26	1.0000	1.0000	0.5567	0.3147
#11	1.0000	1.0000	0.6789	0.4719	#27	1.0000	1.0000	0.6292	0.2614
#12	1.0000	1.0000	0.6895	0.4721	#28	1.0000	1.0000	0.6547	0.3058
#13	1.0000	1.0000	0.6954	0.4374	#29	1.0000	1.0000	0.6587	0.3287
#14	1.0000	1.0000	0.7045	0.5023	#30	1.0000	1.0000	0.7174	0.5289
#15	1.0000	1.0000	0.7125	0.4921	#31	1.0000	1.0000	0.7199	0.5465
#16	1.0000	1.0000	0.7214	0.4985	#32	1.0000	1.0000	0.7347	0.5522
#17	1.0000	1.0000	0.7165	0.4969	#33	1.0000	1.0000	0.7525	0.5363

Table VI. Individual relative error of the first seven moments of the 18-node voltage magnitude.

Scenarios/ Error (%)	$\varepsilon_{\alpha^{1}_{7_{u_{18,10\text{-}min_{11:55\text{-}12:05}}}}}$	$\varepsilon_{\alpha^{11}_{7_{u_{18,10\text{-}min_{11:55\text{-}12:05}}}}}$	$\varepsilon_{\alpha^{111}_{7_{u_{18,10\text{-}min_{11:55\text{-}12:05}}}}}$	$\varepsilon_{\alpha^{1111}_{7_{u_{18,10\text{-}min_{11:55\text{-}12:05}}}}}$	$\varepsilon_{\alpha^{11111}_{7_{u_{18,10\text{-}min_{11:55\text{-}12:05}}}}}$	$\varepsilon_{\alpha^{111111}_{7_{u_{18,10\text{-}min_{11:55\text{-}12:05}}}}}$	$\varepsilon_{\alpha^{1111111}_{7_{u_{18,10\text{-}min_{11:55\text{-}12:05}}}}}$
#1	0.055	1.169	1.777	2.365	2.299	1.240	3.756
#2	0.067	1.454	2.217	2.852	2.527	1.626	4.706
#3	0.076	1.617	2.418	3.268	2.756	1.762	5.236
#4	0.087	1.832	2.762	3.748	3.179	2.037	6.125

Table VII. Run time comparison.

Scenarios		#1	#2	#3	#4	#5
Computation time (s)	PPM	0.151	0.171	0.189	0.192	0.246
	MCS	159.02	201.13	227.17	241.12	315.19

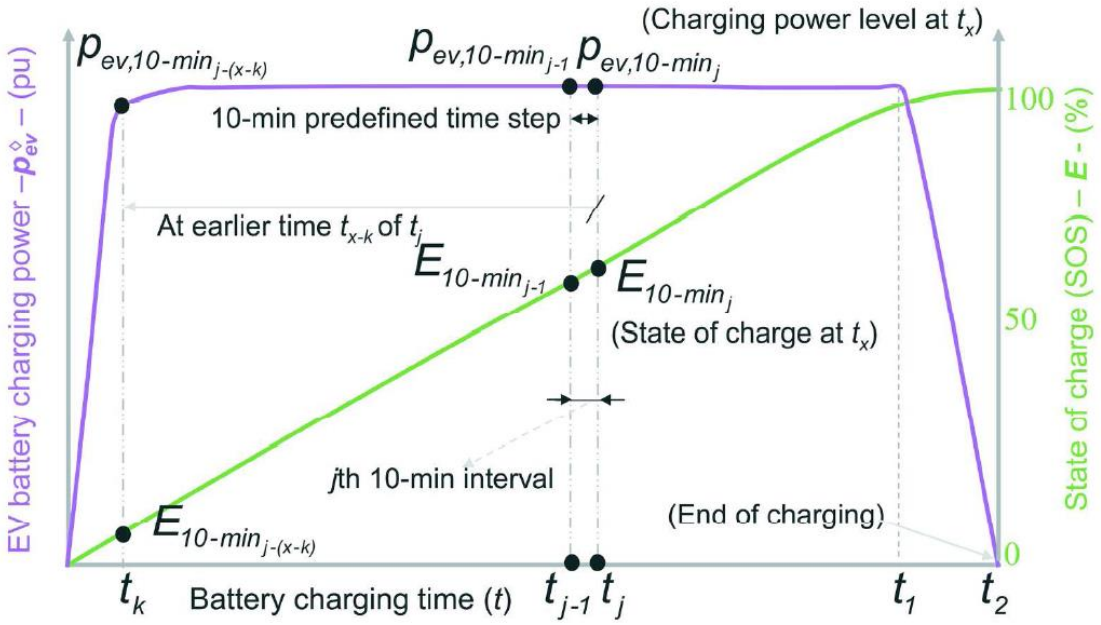

Figure 1. Generic charging profile and SOC for lithium-ion batteries.

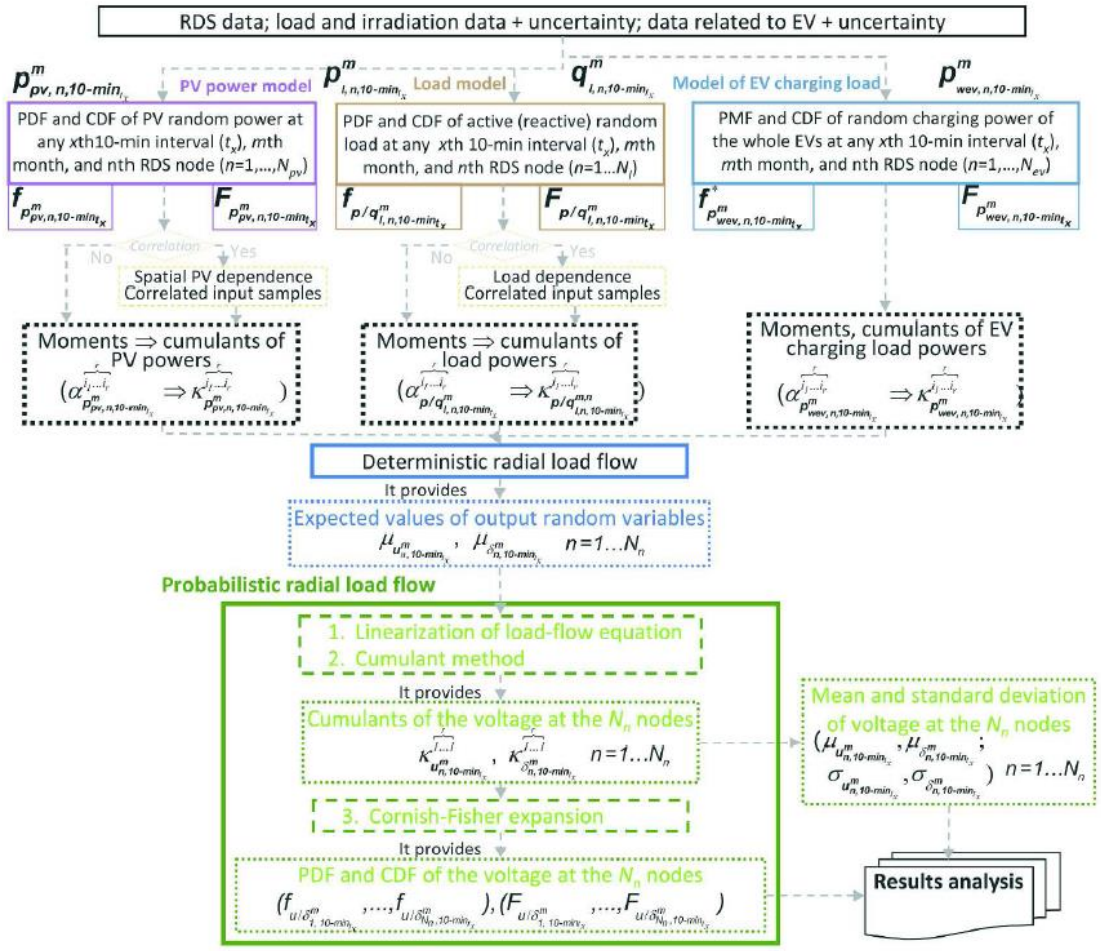

Figure 2. Flowchart of the PPM to assess the impact of PV systems and EVs on RDSs.

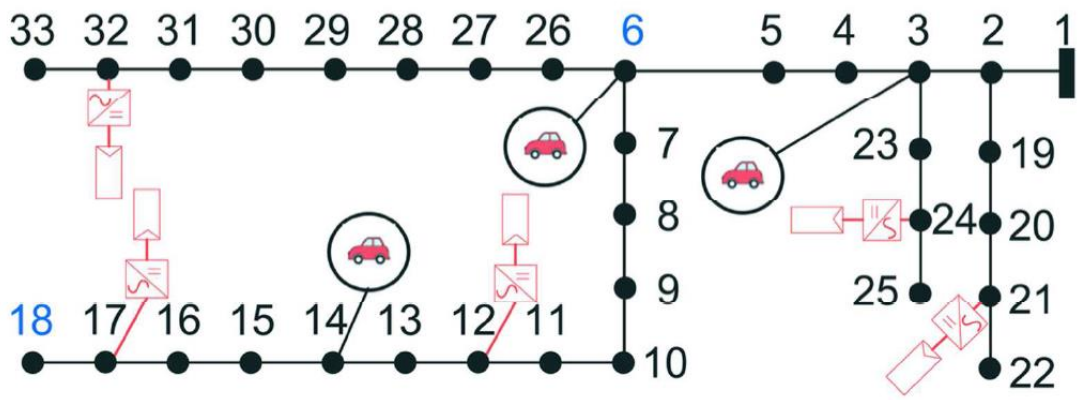

Figure 3. Single-phase diagram of the IEEE 33-node RDS with PV systems and added EVs.

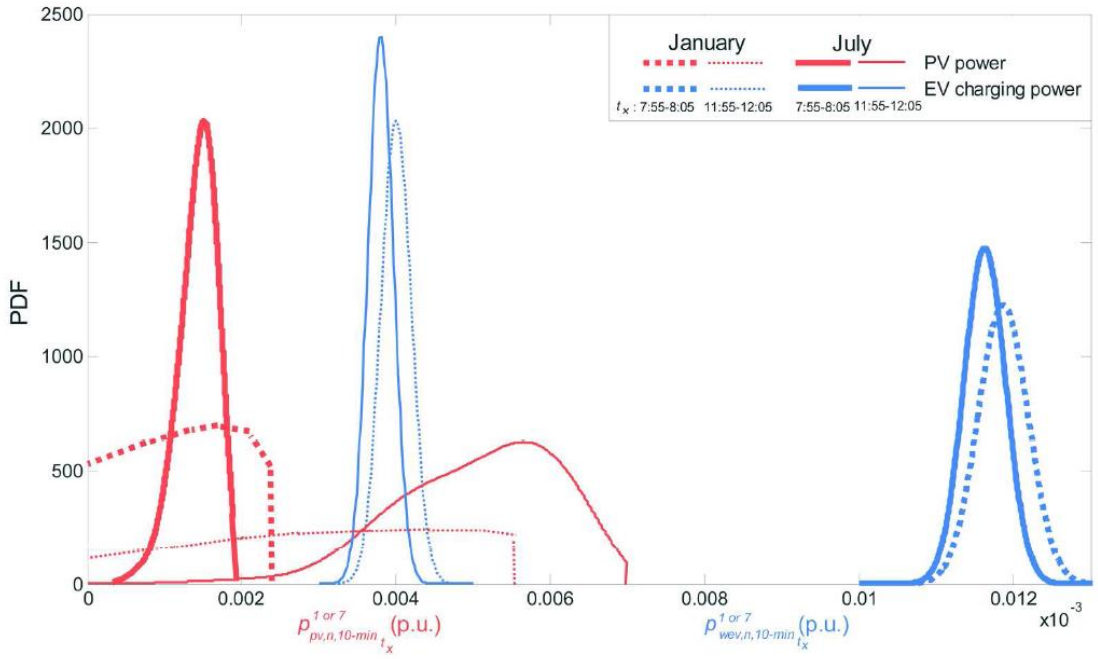

Figure 4. PDFs of PV power and charging power of all of the EVs.

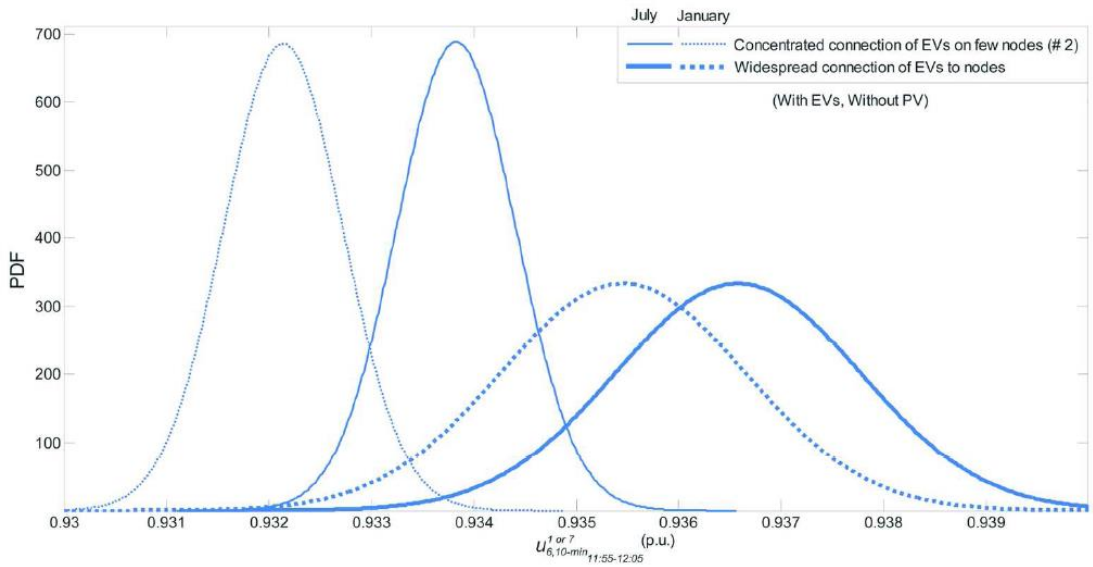

Figure 5. PDF of the 10-min voltage magnitude at noon for node #18 in the defined scenarios.

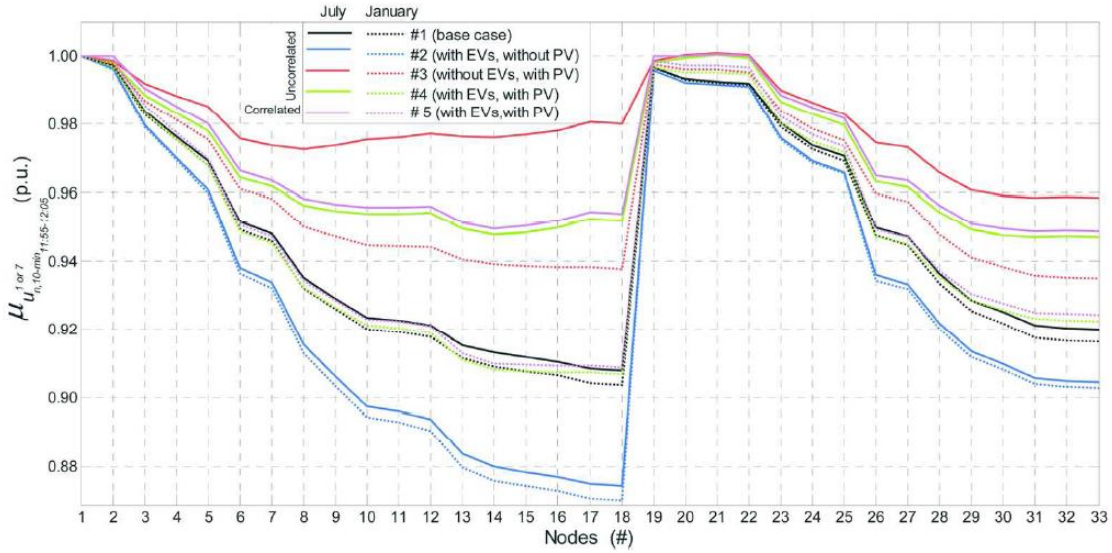

Figure 6. Expected value of the 10-min voltage magnitude at noon for each RDS node in different scenarios.

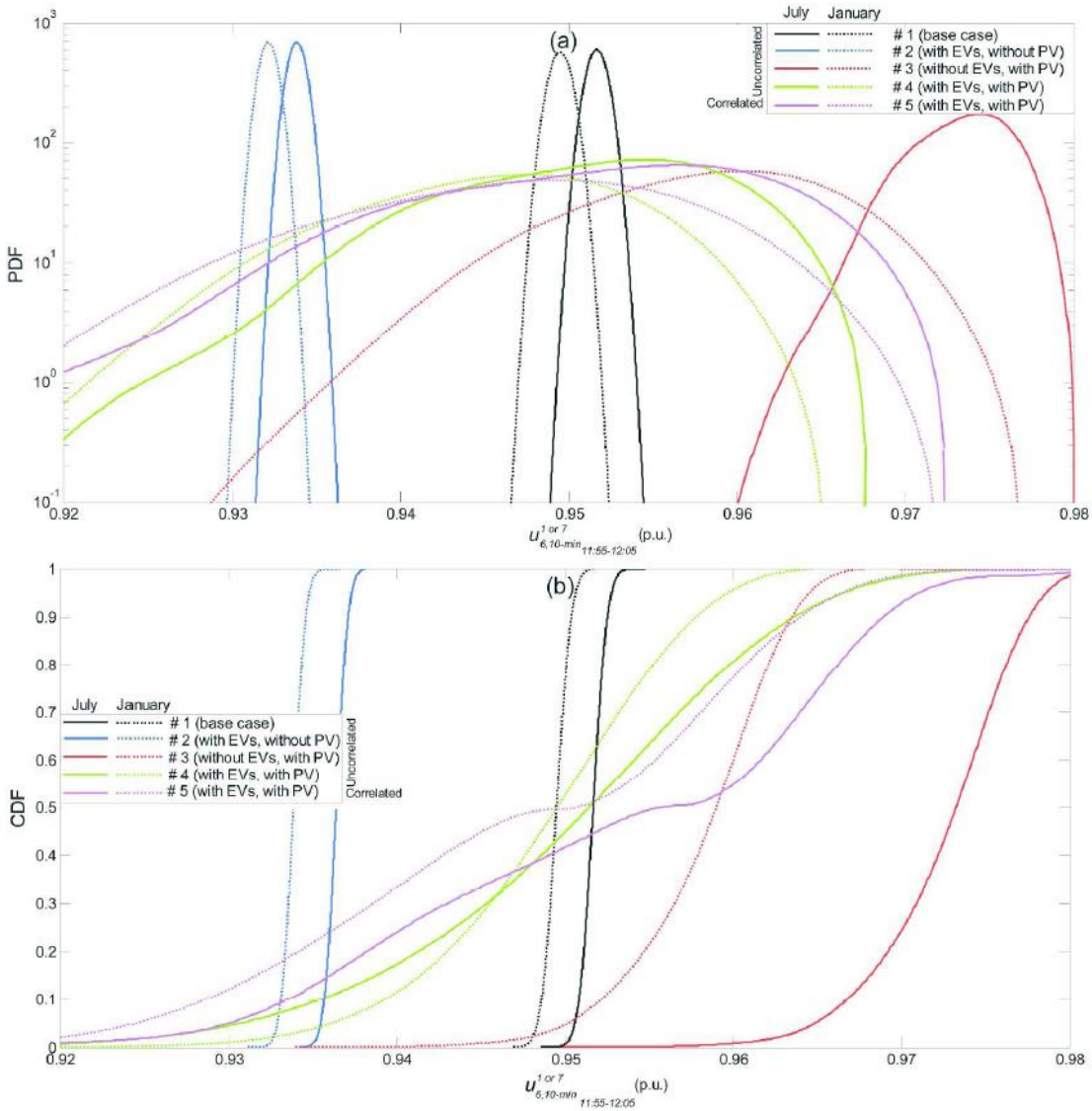

Figure 7. PDF and CDF of the 10-min voltage magnitude at noon for node #6 in the defined scenarios.

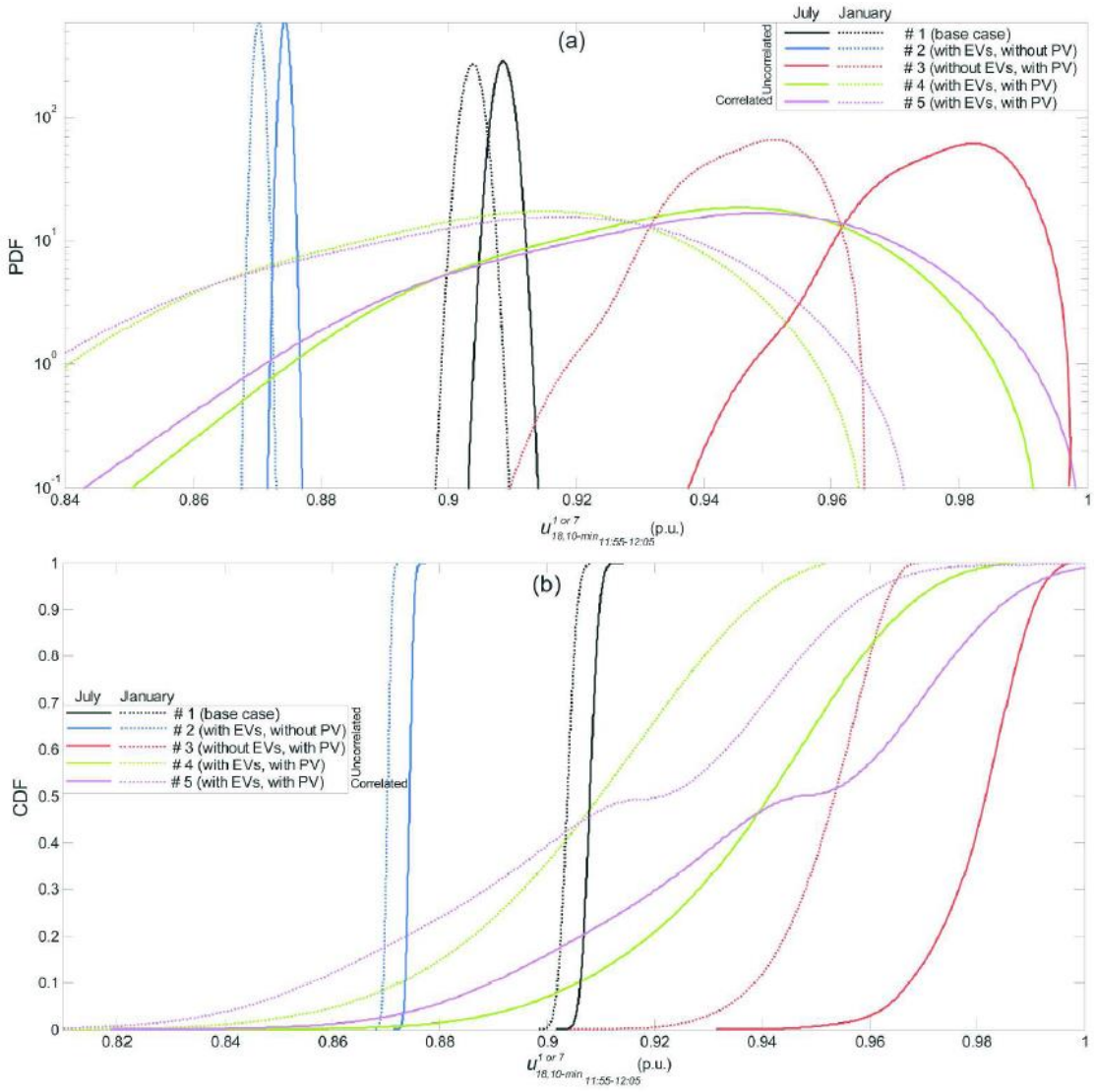

Figure 8. PDF and CDF of the 10-min voltage magnitude at noon for node #18 in the defined scenarios.